Subsurface magnetostratigraphy of Pleistocene sediments from the Po Plain (Italy): Constraints on rates of sedimentation and rock uplift

Giancarlo Scardia†
Dipartimento di Scienze Geologiche e Geotecnologie, Università di Milano-Bicocca, Piazza della Scienza 4, 20126 Milano, Italy, and Alpine Laboratory of Paleomagnetism (ALP), via Madonna dei Boschi 76, 12016 Peveragno (CN), Italy

Giovanni Muttoni
Dipartimento di Scienze della Terra, Università di Milano, Via Mangiagalli 34, 20133 Milano, Italy, and Alpine Laboratory of Paleomagnetism (ALP), via Madonna dei Boschi 76, 12016 Peveragno (CN), Italy

Dario Sciunnach
Regione Lombardia, Geological Mapping Unit, Via Sassetti 32/2, 20124 Milano, Italy

ABSTRACT

We used facies analysis to reconstruct the Pleistocene sedimentary evolution of seven cores from the central-northern Po Plain, Italy. The cores record an overall regressive sequence consisting of shallow-water marine and fluvial-deltaic deposits overlain by fully continental sediments. We used magnetostratigraphy to date marine and fluvial-deltaic sediments to the early Pleistocene and continental sediments to the middle–late Pleistocene. Sediment accumulation rates were ~30–40 cm/k.y. in the early Pleistocene, whereas relevant unconformities and/or an overall reduction in sediment accumulation rates characterized the middle–late Pleistocene. A simple Airy compensation model was applied to restore actual sediments elevations to elevations at times of deposition expressed in meters above current sea level. The correlation of isostatically corrected sedimentary facies to a sea-level curve obtained from classic oxygen-isotope studies shows that an event of rock uplift on the order of ~70–120 m occurred in the middle–late Pleistocene. Literature studies of vegetational cyclicity, used in conjunction with the sea-level curve, allowed us to link sedimentary facies to climate variability. We propose that the onset of fully and persistently continental sedimentation occurred in response to the waxing of the first major Pleistocene glaciation in the Alps, currently correlated to marine isotope stage 22 at ca. 0.87 Ma, and that the episode of uplift occurred (at least in part) as a consequence of erosion and crustal rebound of the Alpine chain triggered by Pleistocene glacial-interglacial cycles.

Keywords: Pleistocene, magnetostratigraphy, Po Plain, Alps, rock uplift, climate variability.

INTRODUCTION

In recent years, there has been much interest in a debate on whether tectonic uplift of mountain belts influenced late Cenozoic global cooling of climate (e.g., Raymo and Ruddiman, 1992), or, if conversely, global cooling and glacial erosion produced isostatic rebound and increased topographic relief (Molnar and England, 1990). We investigated the impact of climate change on erosion and the creation of relief in the Po Plain—the foreland basin of the Alpine-Apennine mountain belt—during the Pleistocene, when the most recent episodes of waxing and waning of Alpine valley glaciers, triggered by enhanced global cooling-warming cycles, left a distinct fingerprint in the sedimentary sequence deposited therein.

Data on the subsurface geology of the Po Plain were gathered since the 1950s by means of seismic surveys and drillings for oil and water exploration, and, in recent years, lithostratigraphic models have been proposed to explain the Pleistocene evolution of the Po Plain (Ori, 1993; Vittori and Ventura, 1995; Pomicino et al., 2001; Carcano and Piccin, 2002; Bini et al., 2004). Moving from this extensive knowledge, we applied magnetostratigraphy to date sedimentary facies of seven cores and link them to climate variability—as revealed by literature estimates of sea-level oscillations—and episodes of vertical tectonic motion in a common evolutionary scenario that shaped the central-northern Po Plain over the last million years.

CORE STRATIGRAPHY

The Geological Survey of Lombardy took seven cores in 1999–2004 from the Po Plain (Fig. 1; Table 1) for a total of 1303 m of recovered sediments (Carcano and Piccin, 2002; this study). Ghedi (RL1), Agrate (RL4), Trezzo (RL5), and Palosco (RL7) (Fig. 2) were drilled along the Southalpine margin between Lake Como and Lake Garda; Pianengo (RL2) and Cilavegna (RL3) (Fig. 3) were drilled more basinward, whereas Cremignane (RL6) (Fig. 3) was drilled in the Sebino glacial complex, south of Lake Iseo. Core stratigraphy typically starts with a cyclic succession of marine fossiliferous silt and very fine-grained bioturbated sand passing upward to medium-grained sand or, at locations more proximal to the Southalpine margin, well-sorted gravel with flat pebbles and ostreids. These thick, shallowing-upward sequences point to deltaic and fan-delta settings cyclically prograding onto a shallow-marine shelf. Upward, the presence of prevailing unfossiliferous clay, silt, and sand arranged in thin fining-upward cyclothems, locally containing abundant peat to gyttja and caliches deposits, points to a distal alluvial-plain environment with cyclically alternating sandy channels and overbank settings. The energy of fluvial transport increases upward, where thicker, fining-upward cyclothems, commonly incomplete, amalgamated, and constituted by medium- to coarse-grained sand, pebbly sand, and gravel,

†E-mail address: giancarlo.scardia@unimib.it.

GSA Bulletin; November/December 2006; v. 118; no. 11/12; p. 1299–1312; doi: 10.1130/B25869.1; 10 figures; 3 tables.

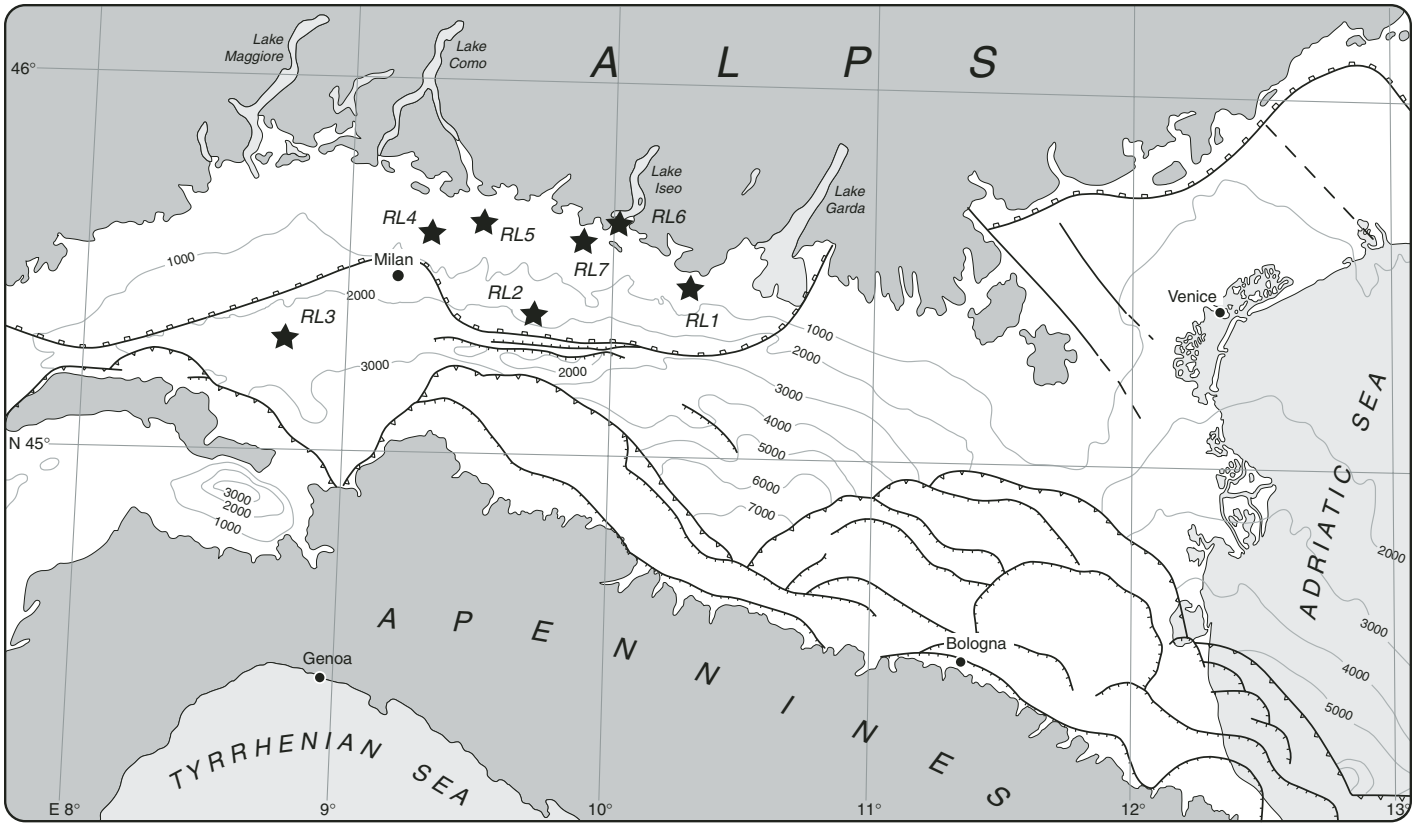

Figure 1. Simplified structural map of the Po Plain with indication of drill sites (Ghedi RL1, Pianengo RL2, Cilavegna RL3, Agrate RL4, Trezzo RL5, Cremignane RL6, Palosco RL7); main buried tectonic elements and the isobaths (m) of the base of the Pliocene–Pleistocene are also indicated (Pieri and Groppi, 1981; Bigi et al., 1990). The Po Plain is shown in white, and the main topographic reliefs are in dark gray.

are interpreted as the expression of a braid plain environment. Exceptions to this general sedimentary pattern are core RL3 (Fig. 3), which is fully continental from its base and records a simple shift from meandering to braided fluvial plains, and core RL6 (Fig. 3), which was drilled into a glacial valley fill that consisted of alluvial fan to glacial deposits.

The occurrence of the calcareous nannofossils normal-sized *Gephyrocapsa* and *G. oceanica* in the lower portion of cores RL2 and RL5 point to a generic Pleistocene age of sediments, whereas a radiocarbon age of 24,024 ± 513 cal yr B.P. was obtained in the uppermost sediments of core RL1. Detailed information on core stratigraphy is summarized in Appendix 1, while information on core recovery is in Table 1; for cores RL1–RL4, see also Carcano and Piccin (2002), and for core RL2, Muttoni et al. (2003).

TABLE 1. CORE DATA AND NUMBER OF PALEOMAGNETIC SAMPLES

Core	Code	Drill site		Altitude	Depth	Core recovery	*N*	*n*	*n/N*
		(°N)	(°E)	(m a.s.l.)	(m)	(%)			(%)
Ghedi	RL1	45°26′57″	10°16′36″	109	201	97	41	37	90
Pianengo†	RL2	45°23′47″	9°42′09″	83	200	94	43	35	81
Cilavegna	RL3	45°18′56″	8°44′05″	115	220	92	36	31	86
Agrate	RL4	45°33′33″	9°21′26″	155	185	90	44	42	95
Trezzo	RL5	45°35′25″	9°30′41″	174	152	87	32	27	84
Cremignane	RL6	45°38′56″	10°00′49″	204	144	84	19	18	95
Palosco	RL7	45°34′43″	9°49′10″	157	201	91	50	44	88

Note: Drill site—latitude and longitude in degrees according to WGS84; altitude in meters above sea level (m.a.s.l.). Depth—total depth of cores from the drill-site surface, in meters. *N*—number of paleomagnetic samples collected; *n*—number of paleomagnetic samples accepted for magnetostratigraphic analyses.
†Paleomagnetic samples from Muttoni et al. (2003).

PALEOMAGNETISM

We studied paleomagnetic properties on a total of 265 cubic samples (~8 cm^3) samples collected from cohesive fine-grained sediments (Table 1). In the upper part of the cores, mostly sandy-gravelly and friable, samples were taken only in the finest-grained levels. The average sampling frequency was on the order of one sample every five core-meters.

Laboratory analyses were conducted at the Paleomagnetic Laboratory of Lamont-Doherty Earth Observatory (cores RL2, RL3, RL5, RL7) and the Alpine Laboratory of Paleomagnetism (cores RL1, RL4, RL6). The natural magnetic remanence (NRM) was measured on a 2G-Enterprises DC squid cryogenic magnetometer located in a magnetically shielded room with ambient fields of ~300 nT. Thermal demagnetization was carried out by adopting a minimum of 10 steps from 100 to 600 °C up to a (rare) maximum of 680 °C. Standard least-square analysis (Kirschvink, 1980) was used to calculate component directions from selected segments of thermal demagnetization diagrams (Zijderveld, 1967). Basic rock-magnetic experiments were

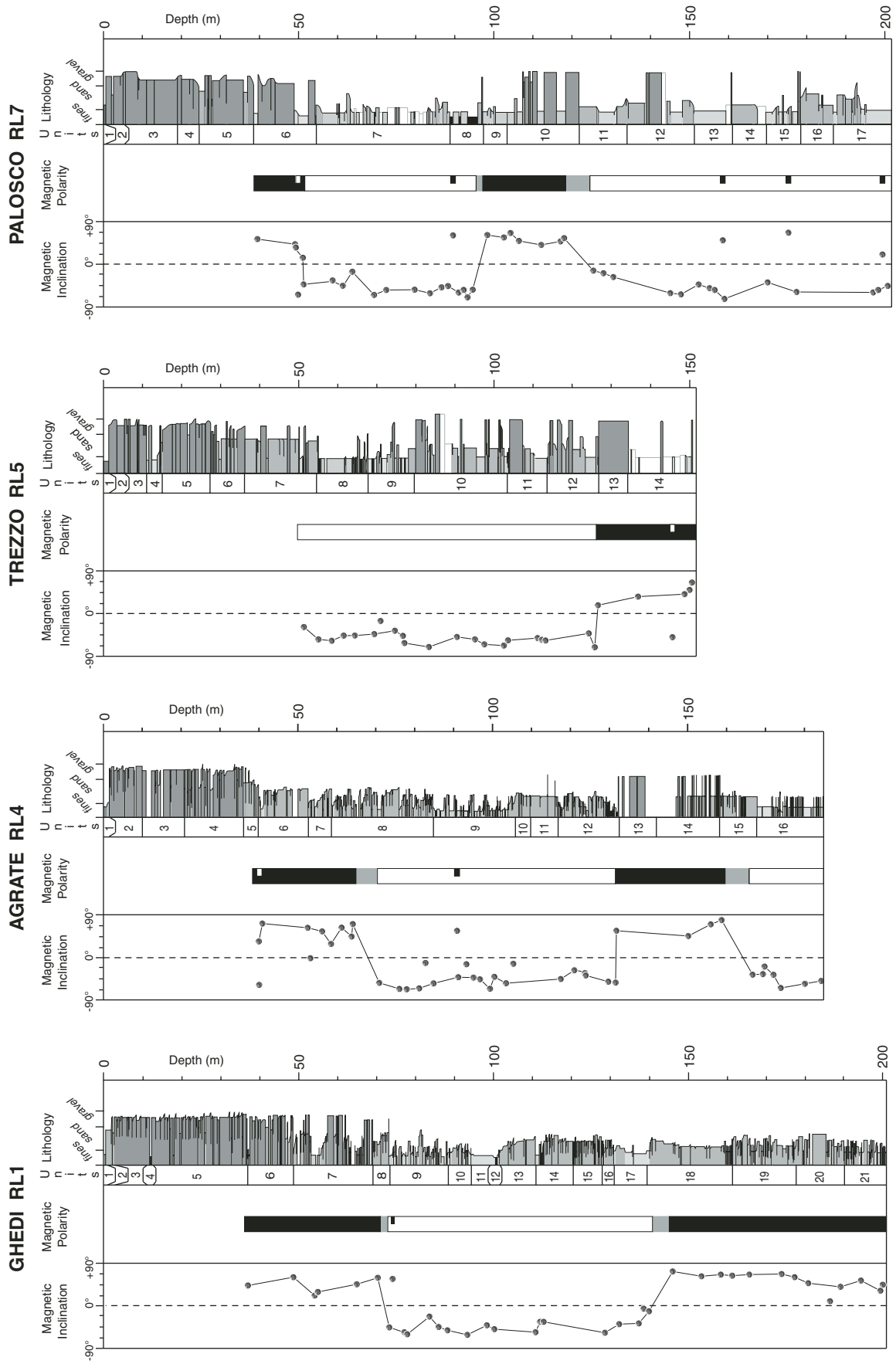

Figure 2. Lithology, stratigraphic units, and magnetostratigraphy of cores Ghedi RL1, Agrate RL4, Trezzo RL5, and Palosco RL7; the magnetostratigraphy was retrieved from the inclination of the characteristic component vectors expressed in degrees from horizontal. Black is normal polarity, white is reverse polarity, and gray is uncertain polarity. See text for discussion.

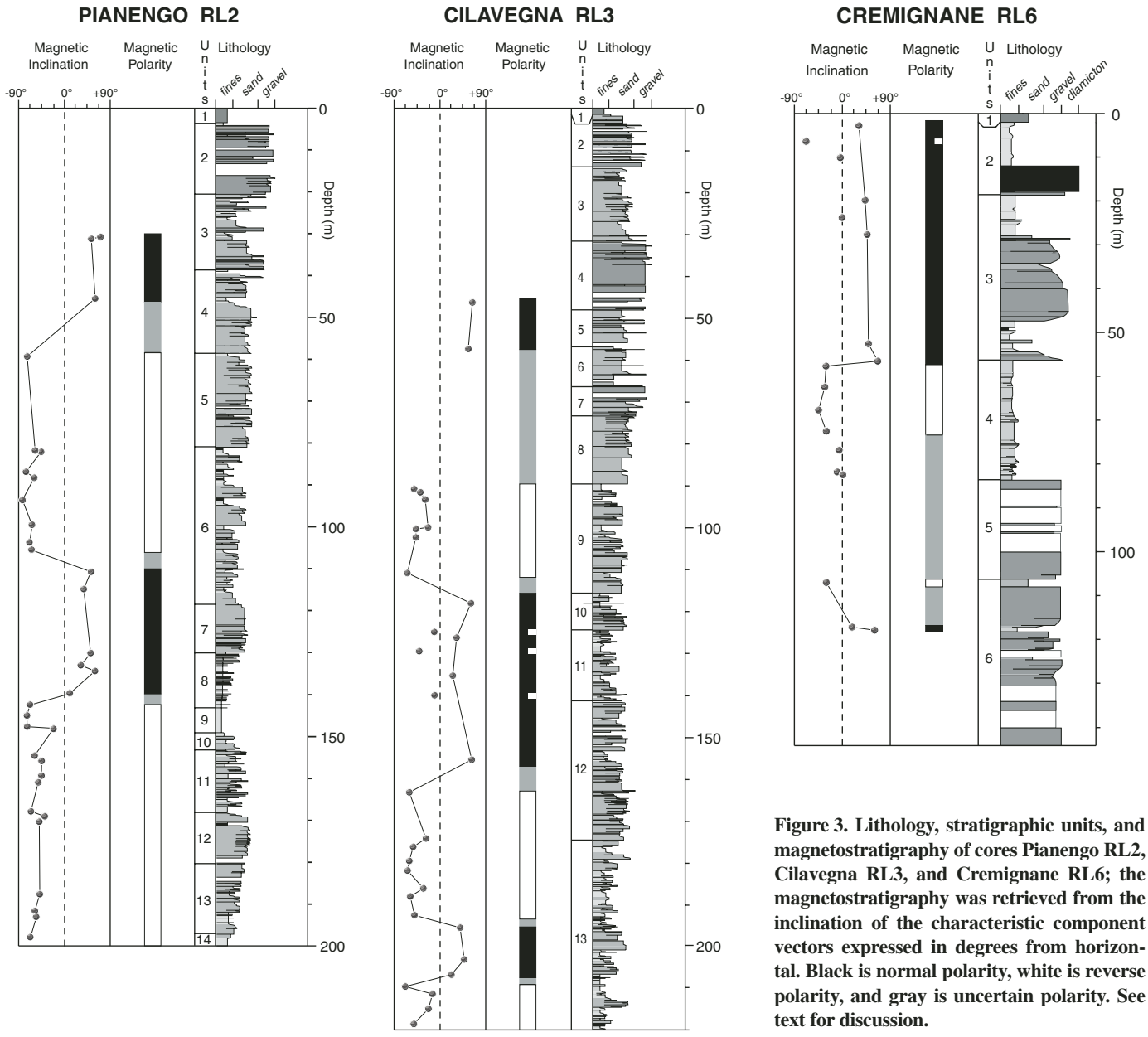

Figure 3. Lithology, stratigraphic units, and magnetostratigraphy of cores Pianengo RL2, Cilavegna RL3, and Cremignane RL6; the magnetostratigraphy was retrieved from the inclination of the characteristic component vectors expressed in degrees from horizontal. Black is normal polarity, white is reverse polarity, and gray is uncertain polarity. See text for discussion.

carried out on cores RL1, RL3, RL5, and RL7; color classes were established by visual comparison with the Munsell Soil Color Chart, and a total of 18 representative samples, an average of 3 per color class, was chosen for isothermal remanent magnetization (IRM) backfield acquisition curves and thermal decay of a three-component IRM (Lowrie, 1990). For IRM acquisition, a 2.5 T field was imparted along a sample axis, then the sample was turned by 180°, and a stepwise magnetization was applied up to 2.5 T. The same sample was successively exposed to 0.4 T and 0.12 T fields along mutually orthogonal axes (as well as orthogonal to the 2.5 T field axis), and was thermally demagnetized.

The intensity of the NRM was on the order of 10^{-2}–10^{-4} A/m. IRM experiments showed the presence of different magnetic carriers and supported a weak dependence of the mineralogical phases on sediment oxidation states as revealed by color analysis. The IRM acquisition of pale-yellow silty clays showed no tendency to saturate even in a field of 2.5 T (Fig. 4, sample RL7–112.1). Thermal decay of the three-component IRM showed that this high-coercivity phase has a narrow spectrum of maximum unblocking temperatures approaching ~680 °C, consistent with detrital hematite as the remanence carrier. The IRM acquisition of pale-yellow clayey silts rose steeply at low fields, but did not reach saturation even at 2.5 T (Fig. 4, sample RL5–124.5). Thermal decay of the soft coercivity fraction showed two moderate intensity falls at ~300 °C and ~570 °C, indicating the presence of an Fe-sulfide phase and magnetite, respectively. The hard- and medium-coercivity fractions showed instead a monotonic decay up to 670 °C and an abrupt fall at 680 °C, typical of hematite. The IRM acquisition of gray silty clays rose initially very steeply and reached ~90% of saturation by 0.3 T, then the curve continued to gently climb up to 2.5 T (Fig. 4, sample RL7–93.3). The medium- and soft-coercivity fractions showed a relevant intensity fall at ~350 °C, indicating the presence of an Fe-sulfide phase,

whereas the small remanence intensity left up to 680 °C, recorded by the hard-coercivity fraction, is indicative of subsidiary amounts of hematite.

Orthogonal projections of demagnetization data typically indicated the existence of a lower unblocking temperature component superimposed onto a higher unblocking temperature component (Fig. 5). The lower unblocking temperature component, removed between room temperature and less than ~300 °C, normally bears steep positive (down-pointing) inclinations, which is thought to be the result of a (sub)-recent magnetization overprint. The higher temperature (characteristic) component was removed to the origin of the demagnetization axes in the magnetite temperature range between ~300 and ~570 °C. Less frequently, maximum unblocking temperatures of 680 °C were reached, consistent with hematite as remanence carrier. This characteristic component bears either positive (down-pointing) or negative (up-pointing) inclinations with overall mean values of 49° ± 16° and –45° ± 16°, respectively, and is regarded as having been acquired at or shortly after sediment deposition.

MAGNETOSTRATIGRAPHY

Cores were not oriented with respect to the geographic north; therefore, only the inclination of the characteristic component vectors was used to outline magnetic polarity stratigraphy. Positive (negative) inclinations were acquired during normal (reverse) polarity of Earth's magnetic field. Polarity intervals were defined by at least three stratigraphically superposed samples. No obvious relationship was observed between magnetic polarity and magnetic mineralogy. We integrated the available biostratigraphic and radiometric data (Appendix 1) with the magnetic polarity stratigraphy interpreted from core tops by comparison with the Cande and Kent (1995) time scale, assuming as a first-order approximation that depth is a linear function of time.

In core RL1, the polarity sequence consists of an upper mainly normal polarity interval interpreted as chron Brunhes (C1n), followed downsection by a predominantly reverse polarity interval interpreted as subchron late Matuyama (C1r.1r), and a lowermost normal polarity interval interpreted as subchron Jaramillo (C1r.1n) (Fig. 2). In core RL2, previous analyses showed a similar polarity sequence extending downsection to reverse polarity subchron middle Matuyama (C1r.2r) (Muttoni et al., 2003; Fig. 3). Similar conclusions were reached for cores RL3 (Fig. 3) and RL4 (Fig. 2). Core RL5 was found to straddle subchron late Matuyama and subchron Jaramillo (Fig. 2), core RL6 chron Brunhes and subchron late Matuyama (Fig. 3), and, finally, core RL7 showed a complete polarity sequence extending from chron Brunhes to subchron middle Matuyama (Fig. 2). Details on the stratigraphic position of polarity reversals are reported in Table 2. From the information outlined here, we derived an internally consistent correlation framework of cores comprehensively spanning an interval of time from chron Brunhes to subchron middle Matuyama (Fig. 6).

AGE-DEPTH FUNCTIONS AND SEDIMENT ACCUMULATION RATES

The available chronological constraints were used to calculate average sediment accumulation rates, taking into account stratigraphic error analysis (Fig. 7; Table 2). Core RL6, proximal to the Pleistocene Sebino glacial complex, was not considered because it showed several sedimentary gaps due to the effects of glacial dynamics.

Uncertainties in age-depth models may derive from sediment swelling and/or liquefaction during core recovery that may alter the location of true depths of stratigraphic surfaces. We estimated these uncertainties to be on the order of only 10 cm, regardless of core length. In addition, because burial compaction may alter original sediment thickness (Allen and Allen, 1990), a decompaction test was performed on the deepest of all cores—RL3—resulting in an overall increase of sedimentary thickness of only 0.7%; we consider this as an upper limit value and explain it with the overall limited burial depth attained by these sediments and the relatively low content of most compressible clay intervals. The most relevant sources of error in estimating sediment age derived essentially from uncertainties in locating accurately the stratigraphic position of polarity reversals, which depended on sampling resolution and the unavoidable necessity of interpolating ages between them and was estimated on the order of ~5 ± 3 m.

In core RL1, chronostratigraphic control points were the radiocarbon age (24,024 ± 513 cal yr B.P.), the Brunhes-Matuyama boundary (B-M, 0.78 Ma), and the top Jaramillo subchron reversal (J_2, 0.99 Ma); sediment accumulation rates were ~35 cm/k.y. in the core section between the B-M and J_2, and minimum rates of ~70 cm/k.y. before J_2 were estimated considering that the core base could not be older than the early Jaramillo subchron reversal (J_1, 1.07 Ma). In core RL2, sediment accumulation rates were ~31 cm/k.y. between the B-M and J_2, and ~37 cm/k.y. between J_2 and J_1. In cores RL3 and RL4, average sediment accumulation rates of, respectively, ~34 and ~33 cm/k.y. were obtained by interpolating all available control

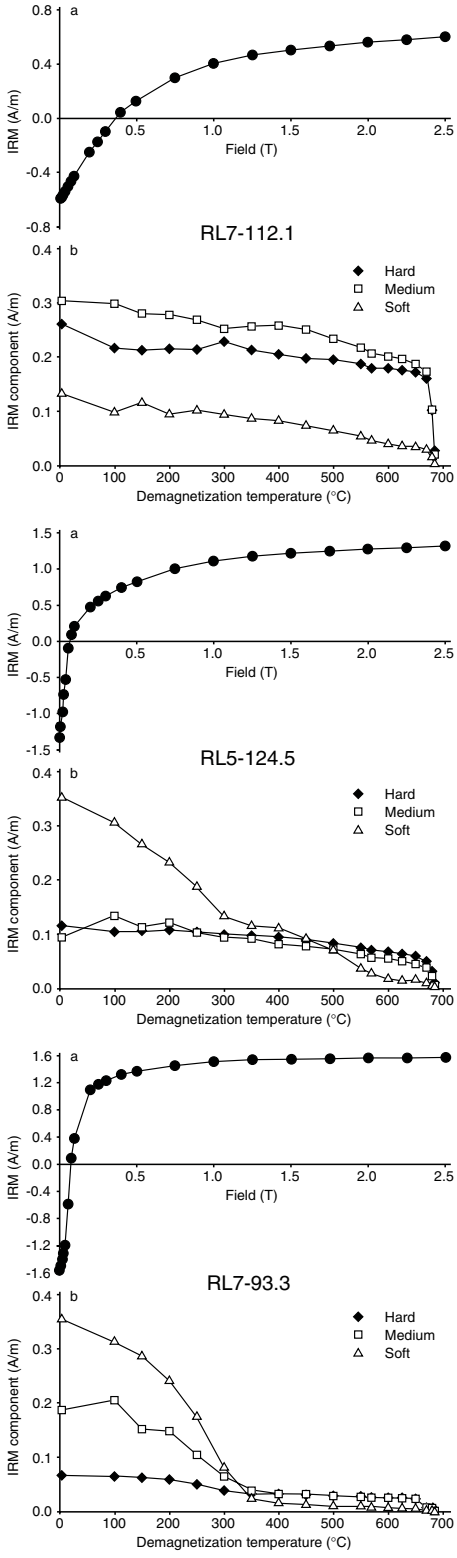

Figure 4. Experiments of isothermal remanent magnetization (IRM) acquisition and thermal demagnetization of a three-component IRM performed on representative samples (identified by the core code and stratigraphic depth). See text for discussion.

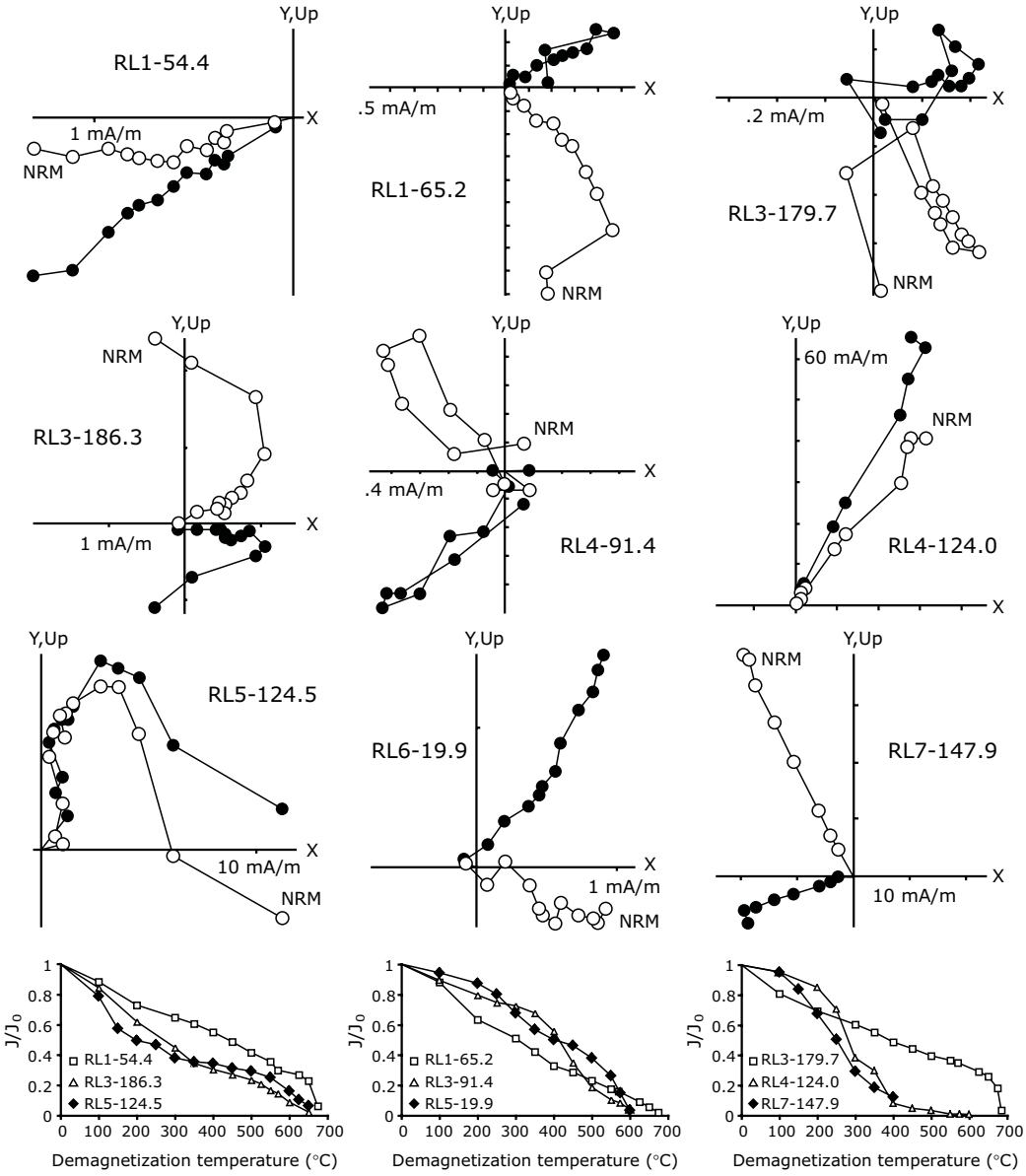

Figure 5. Examples of Zijderveld demagnetization diagrams and normalized (J/J_o) thermal demagnetization curves of natural remanence magnetization (NRM). Open (closed) symbols are projections onto the vertical (horizontal) plane. Horizontal projections have arbitrary azimuths, as cores were not oriented with respect to the geographic north. Samples are identified by the core code and stratigraphic depth.

TABLE 2. CHRONOSTRATIGRAPHIC CONSTRAINTS IN CORES

Depth in core (m)						Age (Ma)	Chronology
RL1	RL2	RL3	RL4	RL5	RL7		
12.0	–	–	–	–	–	0.024	^{14}C cal yr B.P.†
73.4	45.5	57.2	64.3	<51.3	51.1	0.780	Brunhes-Matuyama‡
–	–	–	–	113.0	–	0.960	~MIS 25/26§
146.6	110.5	118.1	132.0	126.0	97.2	0.990	Jaramillo, top‡
>201.0	139.9	155.6	159.2	>152.0	121.9	1.070	Jaramillo, base‡
–	–	195.7	–	–	–	1.201	Cobb Mt., top‡
–	–	207.0	–	–	–	1.211	Cobb Mt., base‡

Note: MIS—marine isotope stage.
†Hughen et al. (2004).
‡Cande and Kent (1995).
§Shackleton (1995).

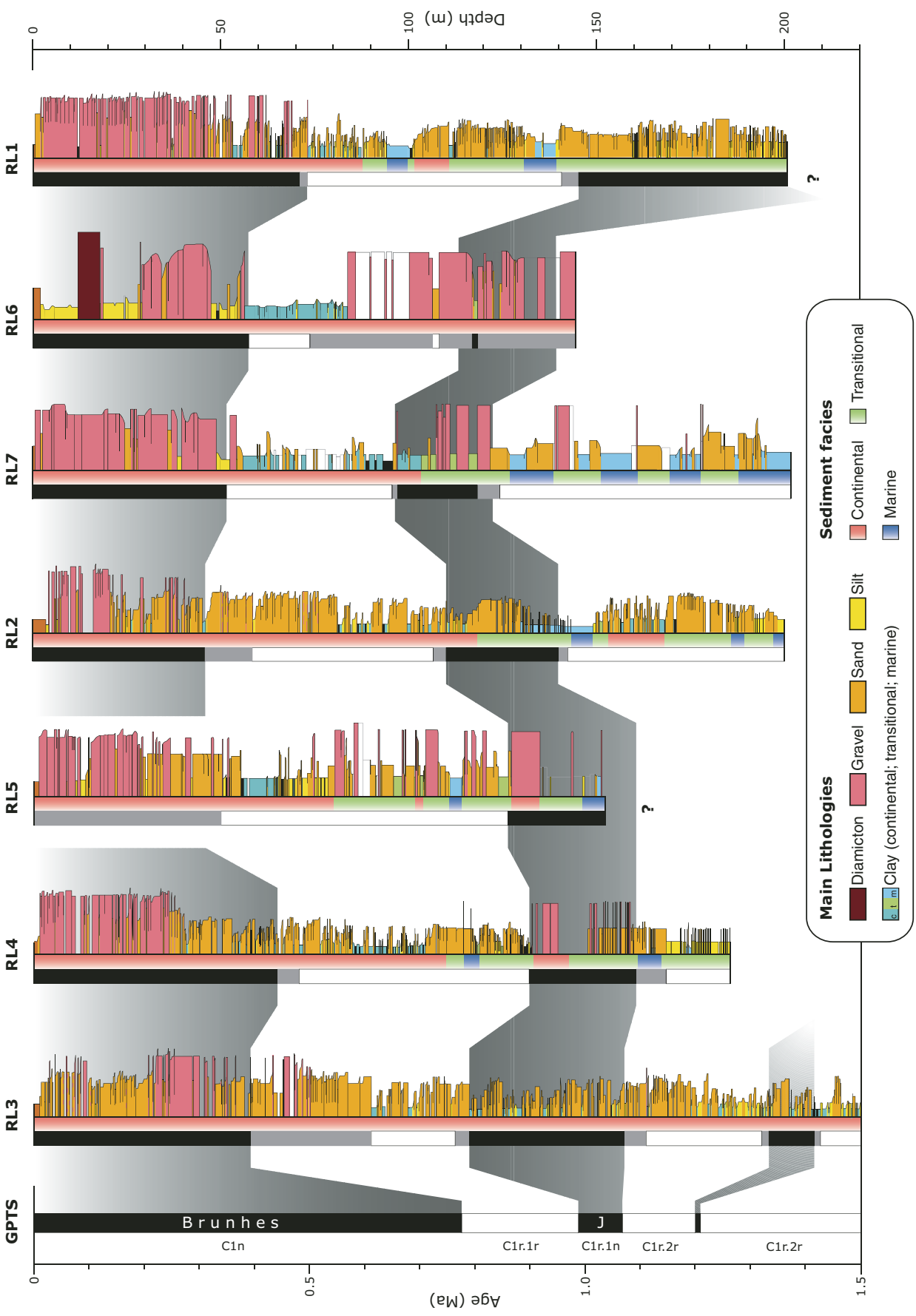

Figure 6. Magnetostratigraphic correlations of the studied cores ordered longitudinally from the west (Cilavegna RL3) to the east (Ghedi RL1). Datum is referred to the ground surface. The geomagnetic polarity time scale (GPTS) adopted for polarity interpretation is that of Cande and Kent (1995).

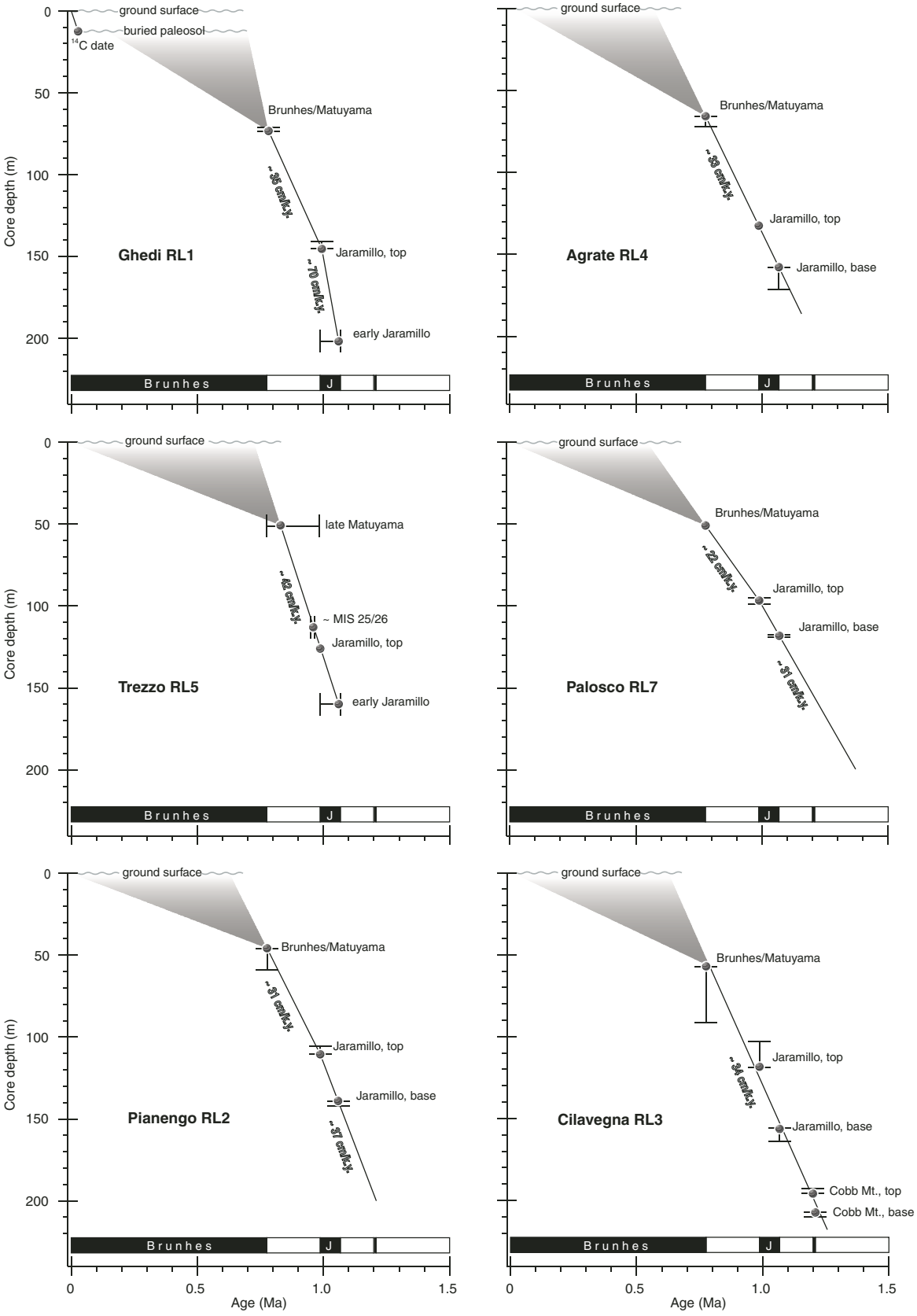

Figure 7. Age versus depth models, constructed for cores Ghedi RL1, Agrate RL4, Trezzo RL5, Palosco RL7, Pianengo RL2, and Cilavegna RL3 by using the available magnetostratigraphic control points and taking into account error analysis. The shaded areas refer to hypothetic age model paths above the Brunhes-Matuyama boundary. MIS—marine isotope stage. See text for discussion.

points between, respectively, the B-M and the Cobb Mountain event (1.201–1.211 Ma), and the B-M and J_1. In core RL5, only one chronostratigraphic control point was available, i.e., J_2; by assuming that marine sediments at 110–113 m were related to the sea-level highstand of marine isotope stage (MIS) 25 (see following discussion), we estimated minimum sediment accumulation rates of ~42 cm/k.y. Finally, in core RL7, average sediment accumulation rates were ~22 cm/k.y. between the B-M and J_2, and ~31 cm/k.y. between J_2 and J_1.

The age of continental sediments deposited during chron Brunhes could be modeled by adopting two extreme hypotheses. By assigning "zero" age to the ground surface, a decrease in sediment accumulation rates to values of ~9–6 cm/k.y. occurred after the B-M boundary. By instead extrapolating the average sediment accumulation rates obtained by the individual age models to ground surface, an age range of ~0.7–0.55 m.y. was obtained for sediments exposed at or immediately below the ground surface. Core RL1, 12 m below ground surface, shows the presence of a buried paleosol older than late Pleistocene (see Appendix 1) overlain by a radiometrically dated ~24-k.y.-old deposit. In the absence of additional chronostratigraphic controls, we explain the limited thickness of continental sediments deposited during chron Brunhes as resulting from reduced accumulation rates and/or the presence of unconformities.

CORRELATION TO THE SEA-LEVEL CURVE AND ESTIMATES OF ROCK UPLIFT

At any time, the vertical motion of a point with respect to sea level depends on the variable contribution of isostasy, tectonics, eustasy, and surface dynamics (England and Molnar, 1990). We notice that in the studied cores, except for core RL2, the uppermost marine intervals lie above present sea level, suggesting an upward vertical motion on the order of 15–60 m (observed rock uplift, Table 3). In order to estimate the relative contribution of isostasy and tectonics to the observed rock uplift and investigate its timing of onset, we applied a simple isostatic compensation model to the calculated age-depth functions and correlated the isostatically corrected sedimentary facies to a recent sea-level curve from the literature. This procedure, substantially similar to that described by Kent et al. (2002), is illustrated as follows by taking core RL1 as a case example (Fig. 8).

1. A reference sea-level curve was constructed by scaling the astronomically tuned ODP677-SPECMAP (Ocean Drilling Program Site 677–Mapping Spectral Variability in Global Climate Project) benthic oxygen-isotope record (Shackleton, 1995) to the 120 m sea-level fall at the Last Glacial Maximum (Fairbanks, 1989).

2. A simple Airy isostatic model was applied to compensate the age-depth function for the effects of sediment load; sediment elevations were backstripped by ~1/3 of overlying sediments thickness (Watts and Ryan, 1976). For example, marine deposits that occurred in core RL1 at 10 m and −30 m above sea level are, after isostatic correction, at 43 m and 16 m, respectively. Details on this procedure are given in Appendix 2.

3. The amount of rock uplift was estimated by studying the position of the backstripped age-depth function relative to the sea-level curve. If the backstripped age-depth function fell into the range of sea-level fluctuations such that the succession of sedimentary facies (marine, transitional, continental) could be appropriately correlated to the sea-level curve of corresponding age, no vertical tectonic motion would have occurred. If instead, as in the case of core RL1, the backstripped age-depth function fell above sea-level fluctuations of corresponding age, rock uplift would have occurred (for completion, if the backstripped age-depth function fell below sea-level fluctuations, tectonic subsidence would have occurred).

4. The amount of rock uplift of core RL1 was estimated by empirically eliminating the displacement between sea-level fluctuations and sedimentary facies of corresponding age; the backstripped age-depth function was "pulled down" vertically by a minimum of 68 m—which represents the minimum amount of rock uplift—such that the succession of sedimentary facies could be readily correlated to the appropriate segment of the sea-level curve.

5. By taking the difference between the age-depth function—corrected for isostasy and rock uplift—and the sea-level curve, an elevation curve in meters above sea level was obtained that visually shows the matching between sedimentary facies and sea-level oscillations (Fig. 9). Inspection of Figure 9 reveals that the younger and older marine deposits of core RL1 correlate to sea-level highstands of MIS 21 (ca. 0.85 Ma) and MIS 25 (ca. 0.95 Ma), respectively. The poor elevation-facies agreement at the core base is attributed to poor control on the (extrapolated) age of sediments down to the J_2 control point.

By using this method, we found rock uplift values of 87 m, 120 m, and 95 m for cores RL4, RL5, and RL7, respectively (Fig. 8). To cross-check the validity of the procedure adopted, we correlated the estimated rock uplift values obtained for each core as described herein to the corresponding values of observed rock uplift derived from the vertical distance between the uppermost marine intervals and present sea level, and found a good agreement (Fig. 10A; Table 3). By correcting the backstripped age-depth functions for the estimated rock uplift values, marine sediments of core RL4 were found to correlate to sea-level highstands of MIS 25 (ca. 0.95 Ma) and MIS 31(ca. 1.07 Ma), and those of core RL5, to MIS 25 and MIS 29 (ca. 1.03 Ma), whereas those of core RL7 correlated to MIS 31 (ca. 1.07 Ma), MIS 35 (ca. 1.18 Ma), and MIS 37 (ca. 1.24 Ma) (Fig. 9). In the most basinward of all cores—RL2—the backstripped elevations of marine sediments at −66 m, −107 m, and −117 m agreed well with sea-level highstands of MIS 31, MIS 35, and MIS 37, respectively, without introducing any vertical tectonic correction (Fig. 9). We infer that rock uplift may have occurred also in core RL2 after an older phase of moderate tectonic subsidence such that a null net difference between subsidence and uplift resulted. Finally, we notice that after the deposition of the youngest marine sediments, which in the studied cores occurred during MIS 25 at ca. 0.95 Ma (locally MIS 21 at ca. 0.85 Ma), fully continental sedimentation was established and persists up to present time.

TABLE 3. OBSERVED AND ESTIMATED UPLIFT VALUES

Core	Uplift (m)	
	Observed	Estimated
RL1	15	68
RL2	–60	~0
RL4	41	87
RL5	64	120
RL7	29	95
Pearson's *r*	0.99†	0.93‡

†Observed versus estimated uplift.
‡Estimated uplift versus latitude; see Table 1 for latitudes.

The age of the rock uplift can be estimated by considering that it should have occurred after the age of the marine-transitional sediments because, if it started before, it would have likely caused them to "lose contact" with sea-level oscillations of typically ~70 m. The rock uplift seems instead temporally associated with the onset of persistent continental deposition after ca. 0.95–0.85 Ma and the generalized reduction of sediment accumulation rates and/or the formation of unconformities during the Brunhes chron (since 0.78 Ma). Causally, the rock uplift may be explained (at least in part) by taking into account the consequences of the onset of the first major Pleistocene Alpine glacial-interglacial cycles at ca. 0.87 Ma, as described in the following section.

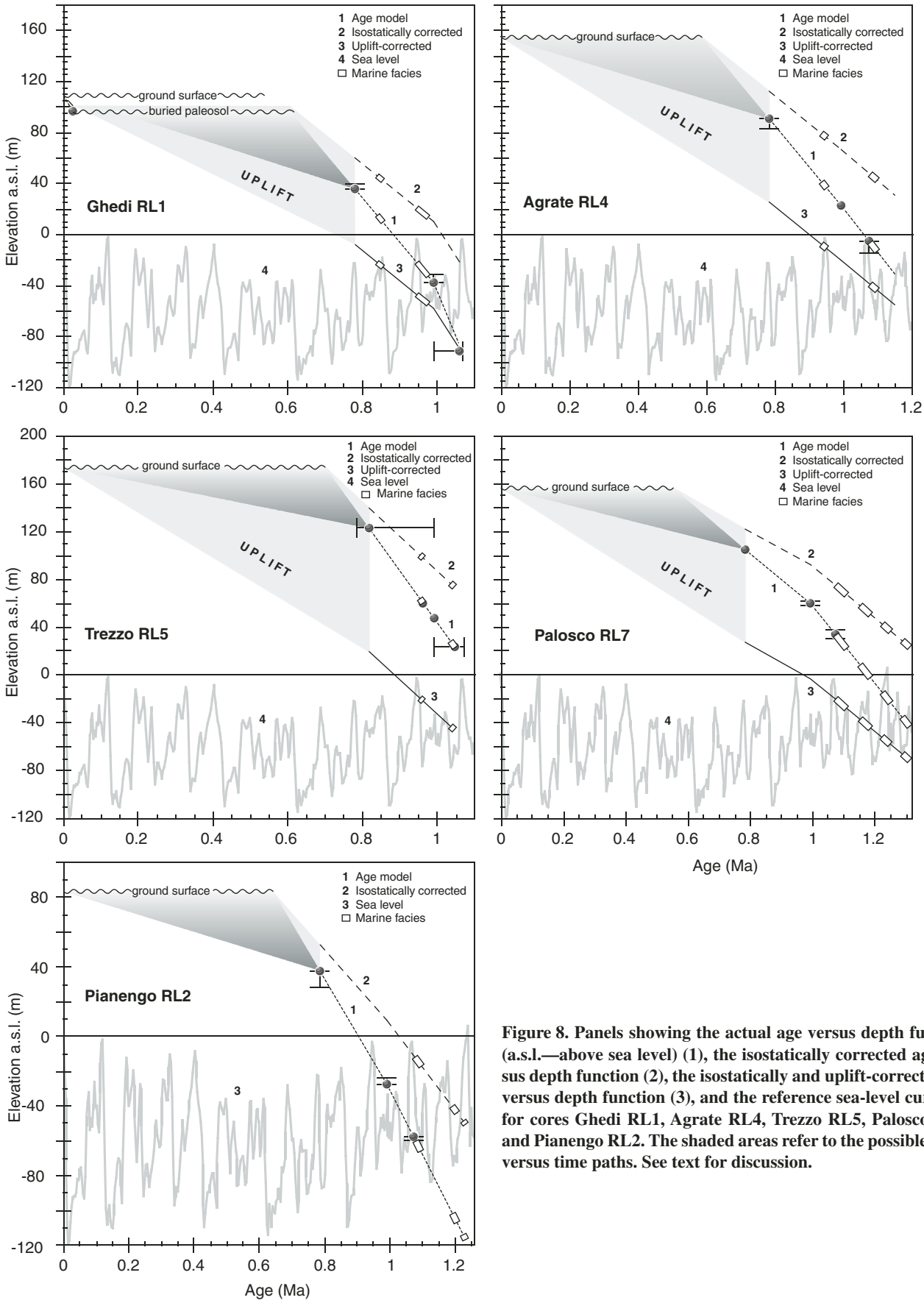

Figure 8. Panels showing the actual age versus depth function (a.s.l.—above sea level) (1), the isostatically corrected age versus depth function (2), the isostatically and uplift-corrected age versus depth function (3), and the reference sea-level curve (4) for cores Ghedi RL1, Agrate RL4, Trezzo RL5, Palosco RL7, and Pianengo RL2. The shaded areas refer to the possible uplift versus time paths. See text for discussion.

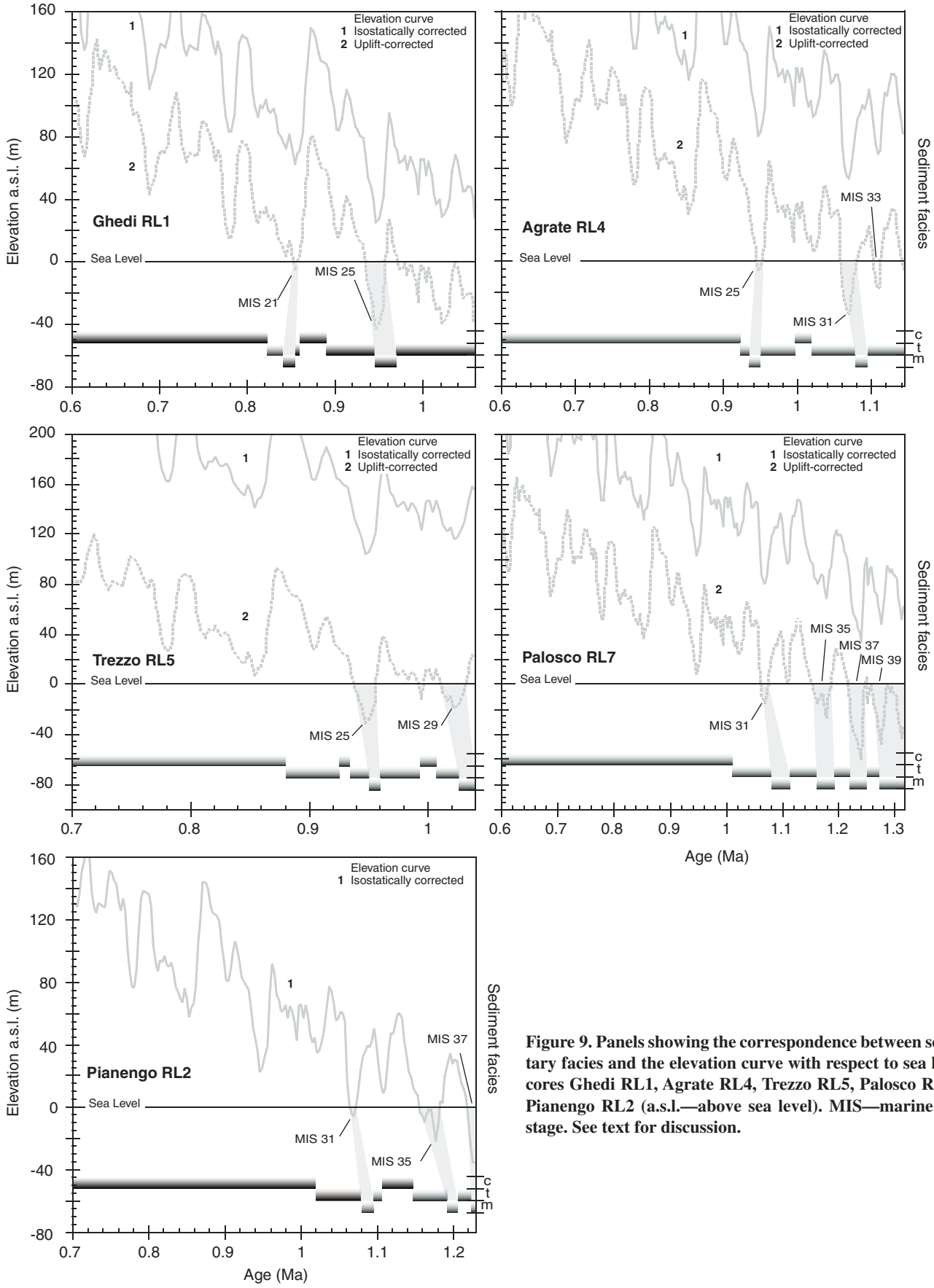

Figure 9. Panels showing the correspondence between sedimentary facies and the elevation curve with respect to sea level for cores Ghedi RL1, Agrate RL4, Trezzo RL5, Palosco RL7, and Pianengo RL2 (a.s.l.—above sea level). MIS—marine isotope stage. See text for discussion.

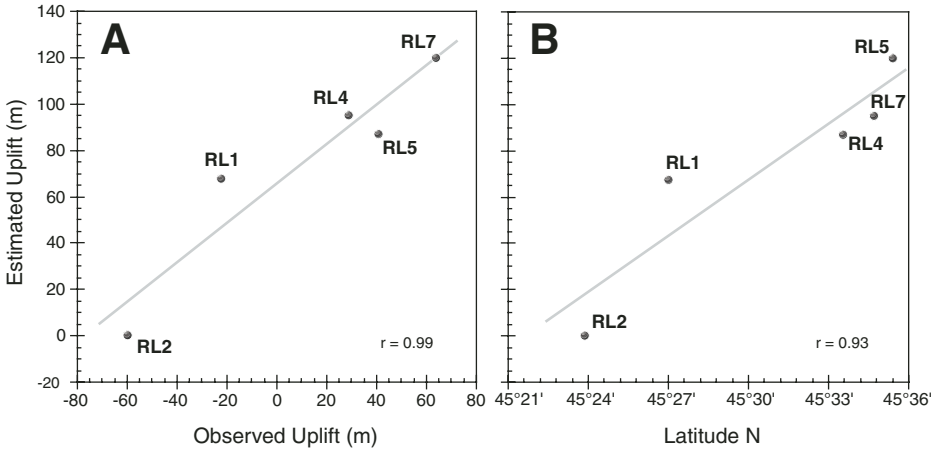

Figure 10. Diagram showing (A) the correlation between observed and estimated rock uplift values for each core (Pearson's correlation coefficient $r = 0.99$; significance level, <1%) and (B) the correlation between latitude (°N) and estimated rock uplift values for each core ($r = 0.93$; significance level <2%). See Figure 1 for core locations and text for discussion.

ICE AGES, EROSION, AND ROCK UPLIFT AT THE FOOTHILLS OF THE SOUTHERN ALPS

The information outlined in the previous sections suggests that a major shift of sedimentation and subsidence styles occurred between the late early Pleistocene and the middle–late Pleistocene. In the late early Pleistocene, marine-transitional deposition occurred at relatively homogeneous sediment accumulation rates of ~30–40 cm/k.y. and was mainly controlled by simple isostatic subsidence. Low-energy meandering fluvial systems sourced in the central Alps flowed W-E toward the northern Adriatic Sea on a low-relief alluvial plain periodically invaded by seawater during the highstands of MIS 37–MIS 25 at ca. 1.24–0.95 Ma; during this time, vegetational analysis from core RL2 and the southern Alps indicates that climate varied cyclically from warm-temperate to cooler but never cold-glacial conditions (Ravazzi and Rossignol Strick, 1995; Muttoni et al., 2003; Muttoni et al., 2006).

The onset of fully continental deposition after ca. 0.95–0.85 Ma broadly coincided with a major shift of Earth's climate variability, indicated in the ODP677-SPECMAP curve by a rapid transition from higher-frequency, lower-amplitude sea-level oscillations typical of the early Pleistocene to lower-frequency, higher-amplitude oscillations typical of the glacial middle–late Pleistocene (Berger et al., 1993). Global cooling climaxed at ca. 0.87 Ma (MIS 22), the first major sea-level lowstand of the Pleistocene, and left a distinct fingerprint in the sedimentary record of the Po Plain and adjacent Southalpine margin, as extensively described in Muttoni et al. (2003). In brief, open vegetation indicating cold climate was established at about this time. Forest withdrawal and sea-level lowstand enhanced erosion on the steep slopes of the Southalpine belt, causing high-energy braided river systems to advance from the Southalpine margin toward the Po Plain, where they triggered the formation of the R surface, an unconformity that can be traced seismically across much of the Po Plain subsurface. This is a candidate time for the Pleistocene Alpine valley glaciers to reach their first maximum southward penetration, with glacier fronts located at the foothills of the southern Alps. Sediments transported southward by braided river systems, as well as glacial sediments transported by Alpine valley glaciers, invaded the Po Plain. Braid-plain progradation coupled with limited (isostatic) subsidence caused coastline retreat. Depositional environments lost contact with the range of sea-level oscillations and became fully and persistently continental.

We propose that the major Pleistocene glacial-interglacial cycles that started in the Alps at ca. 0.87 Ma and continued during chron Brunhes triggered a long-term component of rock uplift in the studied area. Mountain glaciers and fluvioglacial systems may be considered among Earth's most effective agents of erosion and sediment transport; removal of sediments occurs unidirectionally from source areas in the glaciated valleys toward deposition areas in the bordering alluvial plains, which, in the case of the Alps, are the Po River Plain in the south and the central European plains in the north. It is also well known that vertical crustal motions are controlled by erosion, whereby removal of crustal mass leads to isostatic rebound and uplift (Molnar and England, 1990; Schlunegger and Hinderer, 2001; Cederbom et al., 2004). A contribution to the rock uplift of the easternmost core RL1 may also derive from compressional deformation propagated from tectonically active regions to the east of Lake Garda (Desio, 1965; Cremaschi, 1987; Galadini et al., 2001), whereas a contribution to the (inferred) rock uplift of the southernmost core RL2 may derive from compressional deformation related to the propagation of Northern Apennine thrust fronts (Pieri and Groppi, 1981; Bigi et al., 1990; Burrato et al., 2004). But the uplift observed in cores RL4, RL5, and RL7 is not associated with any recognized compressional structure, and may therefore be isostatic in origin. As a final proof of a causative link between erosion induced by glacial-interglacial cycles and rock uplift, we observe that uplift values increase broadly linearly from the (buried) Southalpine front in the south to the chain axial sector in the north (Fig. 10B). This is more consistent with a generalized isostatic uplift of the Alpine range, which we expect to be more pronounced toward the chain core, rather than with local activity of buried thrust fronts, which we expect to be more active at the chain front.

CONCLUSIONS

By integrating facies analysis, magnetostratigraphy, and estimates of sea-level oscillations, we linked sedimentation and tectonics to climate variability in the central-northern Po Plain and adjacent Southalpine margin during the early–late Pleistocene. Climate controlled the actual distribution of early Pleistocene depositional facies on a low-relief, isostatically subsiding alluvial plain where coastlines oscillated cyclically in phase with global ice-volume variations. It controlled sediment source by determining the type of surface weathering and erosional processes, amount and type of vegetation and soil cover, and hydraulic regime of fluvial systems. It may have finally controlled the onset of a period in the middle–late Pleistocene dominated by crustal rebound and uplift, which we attribute (at least in part) to increasing rates of erosion during the waxing and waning of major Alpine valley glaciers. Paraphrasing Molnar and England (1990), we conclude that climate change, weathering, erosion, and isostatic rebound interacted in a system of positive feedback.

APPENDIX 1. CORE LITHOSTRATIGRAPHY

Ghedi RL1 (Fig. 2)

The core starts at the base with fine-grained sands with silty clays (units 21–19, deltaic) passing to very fine-grained sands (unit 18, littoral).

Marine fossiliferous silty clays with very fine-grained sands (units 17, shelfal) are overlain by sandy facies with intercalations of silty clays and organic-rich layers interpreted as a prograding delta (units 16–15, prodelta; unit 14, delta front and delta plain). Upward, the first continental conditions are recorded by the sandy infill of a fluvial channel (unit 13). Next, a transgressive sequence is recorded by silty clayey facies (unit 12, littoral) passing into massive fossiliferous clays (unit 11, lagoon/shelf). A new regressive sequence starts above this and has very fine-grained sands with clayey layers (unit 10, deltaic) overlain by fully continental fine-grained sands with organic-rich layers (unit 9, alluvial plain). With unit 8, fluvial sediments become progressively coarser grained. A relevant discontinuity was recognized at 12.4 m at the top of unit 5, where a strongly rubefied paleosol with pedogenetic features older than late Pleistocene (Cremaschi, 1987) developed and was partially eroded and overlain by an organic-rich clay layer interpreted as a marshy deposit (unit 4). Radiocarbon dating of sediments of unit 4 yield a value of 21,390 ± 230 yr B.P. (24,024 ± 513 cal yr B.P.; Hughen et al., 2004).

Agrate RL4 (Fig. 2)

The core starts at the base with a 45-m-thick coarsening-upward sequence dominated by clayey silts that passes to sands and gravel-dominated deposits (units 16–13, prograding fan-delta). A regressive sequence consisting of coarsening-upward cycles of silts and sands follows (unit 12, prodelta; unit 11, delta front) and passes to sands (unit 10, alluvial plain channel) and organic-rich silty clays (unit 9, overbank). Next, units 8 and 7 consist of very fine- to medium-grained, cross-bedded sands with fining-upward cycles of meandering channel facies. Next, massive to cross-bedded, coarse-grained sands (unit 6) and sandstones (unit 5) pass to polygenetic gravel-dominated deposits (units 4–2, braid plain).

Trezzo RL5 (Fig. 2)

The core starts at the base with gravels and thin layers of fossiliferous silty clays (units 14–13) attributed to a regressive sequence within a fan-delta progradation. Next is a transitional sequence consisting of coarsening-upward cycles of silty sands and gravels (unit 12). This is overlain by a new regressive sequence, which consists of marine fossiliferous silts (unit 11) that pass to coarsening-upward cycles of gravels that include reworked ostreids (unit 10). Next follow peat layers (unit 9) that are interpreted as an upper delta plain overlain by continental sediments. Unit 8 consists of silty layers with abundant organic matter interpreted as an overbank sequence overlain by the gravelly sands of unit 7. Upward, normally graded sandy gravels with sandy layers (unit 6) pass into higher-energy conglomerates (unit 5, braid plain) and are overlain by poorly sorted silty sandy gravels and conglomerates (unit 4–2). The following Pleistocene nannofossils were recovered: *Gephyrocapsa muellerae*, *G. ericsonii*, *Reticulofenestra* sp., and *Syracosphaera pulchra* at 150.2 m (unit 14); *Sphenolithus abies*, *Gephyrocapsa ericsonii*, and *Coccolithus pelagicus* at 125.4 m (unit 12); *Gephyrocapsa ericsonii* and *G. oceanica* at 110.5 m (unit 11); *Reticulofenestra* sp., *Gephyrocapsa ericsonii*, and *Helicosphaera inversa* at 90.4 m (unit 10).

Palosco RL7 (Fig. 2)

The core starts at the base with marine fossiliferous and bioturbated silts with subordinate fine-grained sands that are overlain by massive silty sands of shelfal origin sealed by gravels forming coarsening-upward and subordinate fining-upward cycles (unit 17–12); coarsening-upward cycles define a regressive trend interpreted as fan-delta progradation. Unit 11 consists of fine-grained silty sands passing into sandy silts and fine-grained sands pertaining to a littoral sequence fining- then coarsening-upward. Next follow fining-upward cycles of sandy gravels and conglomerates sealed by silts pertaining to a new fan-delta succession (unit 10). Unit 9 consists of a coarsening- then fining-upward sequence interpreted as a deltaic progradation and abandonment followed by sandy silts and organic-rich clays of meandering alluvial plain origin (unit 8). Silt to sand deposits with organic layers follow (unit 7, meandering alluvial plain) and are abruptly overlain by coarser-grained sediments (units 6–2, braid plain).

Pianengo RL2 (Fig. 3)

The core shows at the base marine fossiliferous silty clays (unit 14, shelfal) passing to very fine– to medium-grained sands (unit 13, littoral to lower shoreface; unit 12, deltaic) overlain by fine-grained sands with organic-rich layers (unit 11, floodplain). Fine-grained silty sands and silty clays follow (unit 10, littoral) and are overlain by marine fossiliferous clays (unit 9, shelfal). Next, a regressive sequence starts with transitional-marine, coarsening-upward silty clays and very fine- to medium-grained sands, which are interpreted as a prograding delta (unit 8, prodelta; unit 7, delta front) overlain by continental very fine- to medium-grained, well-sorted, cross-bedded sands (unit 6, meandering fluvial channel and crevasse-splay sequences). At 80.8 m from the ground level, a prominent facies boundary is recorded. This boundary, called R surface, is marked by an increase of medium- to coarse-grained, poorly sorted pebbly sands and sandy gravels derived from high-energy fluvial systems (units 5–2, braid plain), the onset of which was related by Muttoni et al. (2003) to the waxing of major Pleistocene glaciations in the Alps. Paleodepths of marine facies intervals, based on benthic foraminifers quantitative analysis (Carcano and Piccin, 2002), are on the order of ~3–7 m (unit 9), ~17 m (or less according to lithofacies analysis; unit 13), and ~10 m (unit 14) and therefore suggest infralittoral environments of deposition. The following Pleistocene nannofossils were recovered (Muttoni et al., 2003): "normal size" *Gephyrocapsa* at 200 m (unit 14); "normal size" and "small" *Gephyrocapsa* at 188 m (unit 13); "normal size" *Gephyrocapsa* at 147.1 m (unit 9).

Cilavegna RL3 (Fig. 3)

The core consists of fully continental deposits. The lower part of the section consists of a thick succession of very fine– to coarse-grained sands with silty clays, silts, and organic-rich layers often arranged in fining-upward cycles (units 13–9, fluvial channel, floodplain, and marshy facies). Coarse-grained sands follow (unit 8, distal braid plain) and are overlain by polygenetic, fine- to coarse-grained gravels and sands (unit 7, proximal braid plain). Next follow gravelly, medium- to coarse-grained and laminated sands (units 6–5, braid plain) overlain by coarse-grained sandy gravels arranged in thick graded layers (unit 4). Upward, massive to laminated, medium- to coarse-grained sands with rare pebbles pass into alternations of thick, poorly sorted, medium- to coarse-grained sands with thin polygenetic sandy gravel beds (units 3–2).

Cremignane RL6 (Fig. 3)

The core starts at the base with a 38-m-thick sequence of dominant matrix-supported conglomerates (unit 6) interpreted as low- to medium-energy alluvial fan deposits. A 23-m-thick sequence of matrix- to clast-supported sandy conglomerates of medium- to high-energy alluvial fan origin follows (unit 5) and is overlain by massive sandy silts with dropstones of glaciolacustrine origin (unit 4). Unit 3 is arranged in four subsequences: massive clayey silts and medium- to coarse-grained sands pass at ~47.5 m to fine-grained gravels with silty sandy matrix arranged in a 7-m-thick coarsening-upward sequence; this is in turn overlain at ~35 m by sandy, coarse-grained gravels and massive clayey silts with dropstones. The whole cycle is interpreted as a fining-upward sequence

related to the waxing and waning of a glacial front. Next is a new glacial cycle (unit 2) made of poorly sorted silty sandy gravels (high-energy fluvial deposits) and diamicton with abundant matrix (lodgment till) passing upward to sandy silty clays with dropstones, interpreted as a glaciolacustrine deposit overlain by weathered massive loess silts.

APPENDIX 2. BACKSTRIPPING

Simple Airy isostatic compensation was applied to backstrip the sediment load effect following equation 1 of Watts and Ryan (1976). A rough density of ~1800 $kg \cdot m^{-3}$ was adopted for the sedimentary sequence of all cores. This was obtained by taking the average between a value of 1990 $kg \cdot m^{-3}$ for gravel- and sand-bearing sediments (calculated by using a density of gravel and sand grains of ~2650 $kg \cdot m^{-3}$ and assuming water-saturated porosity of 40%; Sclater and Christie, 1980) and a value of 1688 $kg \cdot m^{-3}$ for mud-bearing sediments (calculated by using a density of mud grains of ~2720 $kg \cdot m^{-3}$ and assuming water-saturated porosity of 60%; Sclater and Christie, 1980). Using the backstripping formula of Sclater and Christie (1980), a rough density of ~1800 $kg \cdot m^{-3}$ results in an ~1/3 increase of sediment thickness due to load-related subsidence, which would need to be removed from the age model.

ACKNOWLEDGMENTS

We thank reviewers C. Langereis and C. Harrison, the associate editor D. McNeill, and editor K. Karlstrom for their very useful comments. The present work would not have been possible without the strong commitment of C. Carcano and A. Piccin in starting a long-term study on the Po Plain subsurface in Lombardy. D. Corbari and S. Miletta helped collecting, organizing, and interpreting stratigraphic data; E. Erba and B. De Bernardi studied the nannofossils association of core RL5; D. Catellani studied the paleodepth data of core RL2; D.V. Kent welcomed Scardia to use his paleomagnetic facility at Lamont-Doherty Earth Observatory and provided a digital listing of the ODP677-SPECMAP (Ocean Drilling Program Site 677–Mapping Spectral Variability in Global Climate Project) data. C. Baroni, A. Bini, P. Burrato, M. Cremaschi, E. Garzanti, D.V. Kent, L. Lanci, and R. Pini are gratefully acknowledged for their useful criticism, comments, and discussions on earlier drafts of this paper.

REFERENCES CITED

Allen, P.A., and Allen, J.R., 1990, Basin analysis: Oxford, Blackwell, p. 451.

Berger, W.H., Bickert, T., Schmidt, H., and Wefer, G., 1993, Quaternary oxygen isotope record of pelagic foraminifers: Site 806, Ontong Java Plateau, *in* Berger, W.H., et al., eds., Proceedings of the Ocean Drilling Program, Scientific Results, Volume 130: College Station, Texas, Ocean Drilling Program, p. 381–395.

Bigi, G., Cosentino, D., Parotto, M., Sartori, R., and Scandone, P., 1990, Structural model of Italy: Firenze, Società Elaborazioni Cartografiche (S.EL.CA.), Consiglio Nazionale della Ricerche Progetto Finalizzato Geodinamica, scale 1:500,000, 9 sheets.

Bini, A., Strini, A., Violanti, D., and Zuccoli, L., 2004, Geologia di sottosuolo nell'alta pianura a NE di Milano: Il Quaternario, v. 17, p. 343–354.

Burrato, P., Ciucci, F., and Valensise, G., 2004, An inventory of river anomalies in the Po Plain, northern Italy: Evidence for active blind thrust faulting: Annals of Geophysics, v. 46, no. 5, p. 865–882.

Cande, S.C., and Kent, D.V., 1995, Revised calibration of the geomagnetic polarity time scale for the Late Cretaceous and Cenozoic: Journal of Geophysical Research, v. 100, p. 6093–6095, doi: 10.1029/94JB03098.

Carcano, C., and Piccin, A., eds., 2002, Geologia degli Acquiferi Padani della Regione Lombardia: Firenze, Società Elaborazioni Cartografiche (S.EL.CA.), 130 p.

Cederbom, C.E., Sinclair, H.D., Schlunegger, F., and Rahn, M.K., 2004, Climate-induced rebound and exhumation of the European Alps: Geology, v. 32, p. 709–712, doi: 10.1130/G20491.1.

Cremaschi, M., 1987, Paleosols and vetusols in the central Po Plain (northern Italy): Milano, Unicopli, 306 p.

Desio, A., 1965, I rilievi isolati della pianura Lombarda ed i movimenti tettonici del Quaternario: Istituto Lombardo, Rendiconti di Scienze A, v. 99, p. 881–894.

England, P., and Molnar, P., 1990, Surface uplift, uplift of rocks, and exhumation of rocks: Geology, v. 18, p. 1173–1177, doi: 10.1130/0091-7613(1990)018<1173:SUUORA>2.3.CO;2.

Fairbanks, R.G., 1989, A 17,000-year glacio-eustatic sea level record: Influence of glacial melting rates on the Younger Dryas event and deep-ocean circulation: Nature, v. 342, p. 637–642, doi: 10.1038/342637a0.

Galadini, F., Galli, P., Cittadini, A., and Giaccio, B., 2001, Late Quaternary fault movements in the Mt. Baldo–Lessini Mts. sector of the Southalpine area (northern Italy): Netherlands Journal of Geosciences, v. 80, no. 3–4, p. 187–208.

Hughen, K., Lehman, S., Southon, J., Overpeck, J., Marchal, O., Herring, C., and Turnbull, J., 2004, ^{14}C activity and global carbon cycle changes over the past 50,000 years: Science, v. 303, p. 202–207, doi: 10.1126/science.1090300.

Kent, D.V., Rio, D., Massari, F., Kukla, G., and Lanci, L., 2002, Emergence of Venice during the Pleistocene: Quaternary Science Reviews, v. 21, p. 1719–1727, doi: 10.1016/S0277-3791(01)00153-6.

Kirschvink, J.L., 1980, The least squares line and plane and the analysis of paleomagnetic data: Royal Astronomical Society Geophysical Journal, v. 62, p. 699–718.

Lowrie, W., 1990, Identification of ferromagnetic minerals in a rock by coercivity and unblocking temperature properties: Geophysical Research Letters, v. 17, p. 159–162.

Molnar, P., and England, P., 1990, Late Cenozoic uplift of mountain ranges and global climate change: Chicken or egg?: Nature, v. 346, p. 29–34, doi: 10.1038/346029a0.

Muttoni, G., Carcano, C., Garzanti, E., Ghielmi, M., Piccin, A., Pini, R., Rogledi, S., and Sciunnach, D., 2003, Onset of major Pleistocene glaciations in the Alps: Geology, v. 31, p. 989–992, doi: 10.1130/G19445.1.

Muttoni, G., Ravazzi, C., Breda, M., Laj, C., Kissel, C., Mazaud, A., Pini, R., and Garzanti, E., 2006, Magnetostratigraphy of the Leffe lacustrine succession (southern Alps, Italy): Evidence for an intensification of glacial activity in the Alps at marine isotope stage 22 (0.87 Ma): Quaternary Research (in press).

Ori, G.G., 1993, Continental depositional systems of the Quaternary of the Po Plain (northern Italy): Sedimentary Geology, v. 83, p. 1–14.

Pieri, M., and Groppi, G., 1981, Subsurface geological structure of the Po Plain (Italy): Rome, Italy, Consiglio Nazionale delle Ricerche Progetto Finalizzato Geodinamica Publication 414, p. 278–286.

Pomicino, N., Bini, A., Violanti, D., Riva, R., and Zuccoli, L., 2001, Geologia di sottosuolo della Pianura Padana compresa tra i fiumi Serio e Brembo: Geologia Insubrica, v. 6, no. 1, p. 113–124.

Ravazzi, C., and Rossignol Strick, M., 1995, Vegetation change in a climatic cycle of early Pleistocene age in the Leffe Basin (northern Italy): Palaeogeography, Palaeoclimatology, Palaeoecology, v. 117, p. 105–122, doi: 10.1016/0031-0182(94)00118-R.

Raymo, M.E., and Ruddiman, W.F., 1992, Tectonic forcing of late Cenozoic climate: Nature, v. 359, p. 117–122, doi: 10.1038/359117a0.

Schlunegger, F., and Hinderer, M., 2001, Crustal uplift in the Alps: Why the drainage pattern matters: Terra Nova, v. 13, p. 425–432, doi: 10.1046/j.1365-3121.2001.00374.x.

Sclater, J.G., and Christie, P.A.F., 1980, Continental stretching: An explanation of the post–mid-Cretaceous subsidence of the central North Sea Basin: Journal of Geophysical Research, v. 85, p. 3711–3739.

Shackleton, N.J., 1995, New data on the evolution of Pliocene climate variability, *in* Vrba, E., et al., eds., Palaeoclimate and evolution, with emphasis on human origins: New Haven, Yale University Press, p. 242–248.

Vittori, E., and Ventura, G., 1995, Grain size of fluvial deposits and late Quaternary climate: A case study in the Po River valley (Italy): Geology, v. 23, p. 735–738, doi: 10.1130/0091-7613(1995)023<0735:GSOFDA>2.3.CO;2.

Watts, A.B., and Ryan, W.B.F., 1976, Flexure of the lithosphere and continental margin basins: Tectonophysics, v. 36, p. 25–44, doi: 10.1016/0040-1951(76)90004-4.

Zijderveld, J.D.A., 1967, A.C. demagnetization of rocks: Analysis of results, *in* Collison, D.W., et al., eds., Methods in palaeomagnetism: Amsterdam, Elsevier, p. 254–286.

Manuscript Received 6 July 2005
Revised Manuscript Received 3 February 2006
Manuscript Accepted 6 April 2006

Printed in the USA